Sensitivity of Tropical Land Climate to Leaf Area Index: Role of Surface Conductance versus Albedo*

Katrina Hales and J. David Neelin

Department of Atmospheric Sciences, and Institute of Geophysics and Planetary Physics, University of California, Los Angeles, Los Angeles, California

Ning Zeng

Department of Meteorology, and Earth System Science Interdisciplinary Center, University of Maryland, College Park, College Park, Maryland

(Manuscript received 7 October 2002, in final form 18 June 2003)

ABSTRACT

Tropical land climate sensitivities to surface properties are studied using an intermediate complexity atmosphere model. The focus here is on land surface vegetation feedbacks to the atmosphere through surface conductance and albedo. Both properties are linked by a parameterization on leaf area index so that their relative impacts can be compared. For a given percent change in leaf area index, it is found that low and moderate vegetation regions such as the Sahel have a higher sensitivity than rain forest regions such as the Amazon in local total precipitation anomaly, as well as fractional change in precipitation. Comparison of sensitivities to changes in surface conductance and albedo shows that neither is negligible and their relative influence differs among local climatic regions, typified by different vegetation types. High precipitation rain forest regions are more influenced by surface conductance due to the large water recycling ratio there, while albedo has a larger influence in arid, low vegetation regions by modifying the energy balance and large-scale atmospheric circulation. In regions of moderate precipitation and vegetation, altered surface conductance and albedo have comparable effects on precipitation. Surface conductance and albedo have opposing effects on surface temperature but surface conductance has the dominant impact on both surface temperature and evapotranspiration.

1. Introduction

While a number of studies have indicated the potential impacts on climate of various land surface properties such as surface albedo, evapotranspiration, and roughness length (Charney 1975; Shukla and Mintz 1982; Dickinson 1992; Sud et al. 1988), the relative importance of these and other land characteristics are still very uncertain. Part of the uncertainty comes from the fact that the sensitivities seem very different at different locations with semidesert regions such as the Sahel much more sensitive to surface energy perturbation than other regions (Cox et al. 2000). General circulation models (GCMs) have been used to explore various land surface change experiments, for example, global vegetation feedbacks (Lofgren 1995a,b), deforestation of the Amazon (Dickinson and Henderson-Sellers 1988; Lean and Warrilow 1989; Shukla et al. 1990; Sud et al. 1988; Zhang et al. 1996), the Maritime Continent (Delire et al. 2001), and desertification in the Sahel region of Africa (Charney et al. 1977; Xue and Shukla 1993; Xue 1997). Such crucial results are poorly understood despite the improved understanding of how these processes influence climate by modifying surface budgets of energy, water, and momentum (Dirmeyer 1992; Zhang et al. 1996; Zeng and Neelin 1999).

These sensitivity studies typically assume a fixed change in a particular surface property such as albedo without having to worry about the changes in other aspects and how they might be related. It is therefore not possible to quantify the relative importance of these processes in such experiments.

On the other hand, more realistic experiments for deforestation (Dickinson and Henderson-Sellers 1988; Lean and Warrilow 1989; Shukla et al. 1990; Sud et al. 1996; Zhang et al. 1996), desertification (Charney et al. 1977; Xue and Shukla 1993), as well as fully interactive land/vegetation models (Zeng et al. 1999; Cox et al. 2000) include simultaneous changes in all the relevant land and vegetation properties. Because of the com-

* Institute of Geophysics and Planetary Physics Contribution Number 5807.

Corresponding author address: Dr. J. David Neelin, Department of Atmospheric Sciences, University of California, Los Angeles, 405 Hilgard Avenue, Los Angeles, CA 90095-1565.
E-mail: neelin@atmos.ucla.edu

plexity of such problems, attention has rarely been paid to further isolating the relative contributions from different processes.

In this paper, we aim at delineating the roles of two major processes: surface albedo and surface conductance (therefore evapotranspiration). Our approach is to model both processes on a key vegetation property, leaf area index (LAI), such that their changes are constrained by the same vegetation process, thus enabling a direct comparison of their relative importance. Sensitivity studies will be conducted for regions characterized by different vegetation types, and therefore climatic regimes, to quantify the geographical dependence of sensitivities to these two processes. The use of intermediate complexity atmospheric and land surface models has enabled us to conduct large ensemble runs to obtain results with statistical significance despite atmospheric internal variability.

2. The model

a. QTCM summary

We have used the Quasi-Equilibrium Tropical Circulation Model (QTCM) of Neelin and Zeng, version 2.2 (Neelin and Zeng 2000; Zeng et al. 2000), to explore the atmospheric response to altered land surface conditions. The QTCM is an atmospheric model of intermediate complexity designed to capture tropical climate behavior. Based on the primitive equations, the QTCM's main simplification (from GCM-type formulation) is the use of tailored basis functions for temperature and winds that allow severe truncation in the Tropics due to assumptions about convective closure. See Neelin and Zeng (2000) and Zeng et al. (2000) for formulation and analysis of simulations using the QTCM. We run the model on a spatial grid from 60°N to 60°S at ''fine'' resolution of 2.8125° in longitude by 1.875° in latitude and ''coarse'' resolution of 5.625° in longitude by 3.75° in latitude.

b. QTCM land surface model and modifications

The simple-land surface model (SLand) is coupled to QTCM (Zeng et al. 2000). SLand is simple compared to recent biophysical land surface parameterizations (Dickinson et al. 1993; Sellers et al. 1996a). It is slightly more complex than the bucket model, since it imitates aspects of the biophysical models, but much simpler than, for example, Xue (1991). The Project for Intercomparison of Land-Surface Parameterization Schemes (PILPS; Henderson-Sellers et al. 1993) has identified the most important aspects of land surface energy and water budgets relevant to feedbacks to the atmosphere. The findings suggest that a relatively simple model approximately captures the primary effects for climate simulation at time scales longer than diurnal and synoptic scales (Koster and Milly 1997). In SLand, we use a thin land surface layer for energy and a much thicker layer to represent root-zone water budget. Since the land heat capacity is small, the thermodynamic budget essentially yields zero net surface flux on time scales much longer than a day. Land albedos are spatially varying, with a climatological seasonal cycle. Sensible heat fluxes are evaluated using the standard bulk formula, while evaporation has a formulation akin to the biophysical models, with a surface resistance similar to a stomatal resistance combined with the effects of root resistance in dry soil conditions (Dickinson et al. 1993). This resistance has a simplified dependence on soil moisture that increases as the soil moisture drops. Interactive soil moisture (W) is calculated for a single soil layer representing the root zone, driven by precipitation (P) minus evaporation and runoff

$$\frac{\partial W}{\partial t} = P - E_I - R_s - E_T - R_g, \qquad (1)$$

where total evaporation

$$E = E_I + E_T \qquad (2)$$

has separate treatment of interception loss (E_I) and evapotranspiration (E_T). The spatial and temporal variability of rainfall and surface properties are important in determining processes such as interception loss, surface runoff (R_s: the fast component), and subsurface runoff (R_g: the slow component). These are parameterized in a way similar to what is used in the more sophisticated land surface schemes, such as Shuttleworth (1988) and Entekhabi and Eagleson (1989), but with simpler statistical assumptions (Zeng et al. 2000). Evapotranspiration is parameterized as

$$E_T = (r_s + r_a)^{-1}\rho_a[q_{\text{sat}}(T_s) - q_a], \qquad (3)$$

where T_s is the surface temperature, ρ_a is air density, q_a is air humidity, q_{sat} is air humidity at saturation, r_a is the aerodynamic resistance (which depends on roughness height and surface winds), and r_s is the surface resistance where

$$r_s = g_s^{-1} \qquad (4)$$

with g_s, surface conductance, parameterized on soil moisture, vegetation type and, LAI as discussed in section 3c.

1) Surface albedo and conductance

In the Zeng et al. (2000) version of the QTCM, albedo was specified by observations or according to surface type. Here we parameterize it based on leaf area index. Albedo varies spatially and over a 12-month climatology, depending largely on leaf area index (except in snow covered regions or areas with very low vegetation). The surface resistance or its inverse, surface conductance, is a combined stomatal and root resistance, which depends on soil moisture and is modified to also depend on LAI and to a lesser degree on vegetation

TABLE 1. Vegetation classification for DeFries and Townsend (1994) in first two columns; corresponding simplified classification in third and fourth columns. Numerous land classifications exist in the literature, here we include numbers used in DeFries and Townshend corresponding to the classifications used in SiB (Dorman and Sellers 1989). Roughness length (fifth column) is from observed (ISLSCP; Sellers et al. 1996a,b) averaged over the corresponding vegetation class region.

Vegetation classification				
DeFries and Townshend		Simplified for QTCM		Roughness length (m)
0	Water	0	Water	0.0024
1	Broadleaf evergreen forest	1	Rainforest	2.86
2	Broadleaf deciduous forest	2	Other forest	0.91
3	Mixed coniferous and broadleaf deciduous forest and woodland			
4	Coniferous forest and woodland			
5	High-latitude deciduous forest and woodland			
6, 8	Wooded c4 grassland	3	Moderate vegetation	0.12
12	Cultivation			
14	C3 wooded grassland			
7	C4 grassland	4	Low vegetation	0.08
9	Shrubs and bare ground			
15	C3 grassland			
10	Tundra	5	Desert and bare ground	0.03
11	Desert and bare ground			
13	Ice			

class. Formulations for surface albedo and conductance are discussed in sections 3b and 3c. For the experiments described in this paper, both surface albedo and surface conductance are modified by prescribed changes in LAI as discussed in section 4.

2) VEGETATION CLASSIFICATION

We expand from the standard QTCM's three land surface types (desert, grass, and forest) to five types based on the International Satellite Land Surface Climatology Project (ISLSCP) vegetation class data of DeFries and Townshend (1994). The 15 classes of DeFries and Townshend were reduced to six types for use in the QTCM. Table 1 shows the original DeFries and Townshend vegetation class [numbered to be consistent with vegetation classes of Dorman and Sellers (1989) simple biosphere model (SiB)] and the corresponding vegetation class used in these studies. Figure 1 shows the vegetation classification map at the higher resolution of the two used in these modeling experiments.

A subset of the ''desert'' region was defined as ''barren ground'' if climatological leaf area index was less than 0.48 for at least 11 out of the 12 months.

Vegetation class is used to assign roughness length. Values of this parameter are based on observed roughness length (Sellers et al. 1996a,b) and shown in Table 1. Observed roughness length was averaged over each

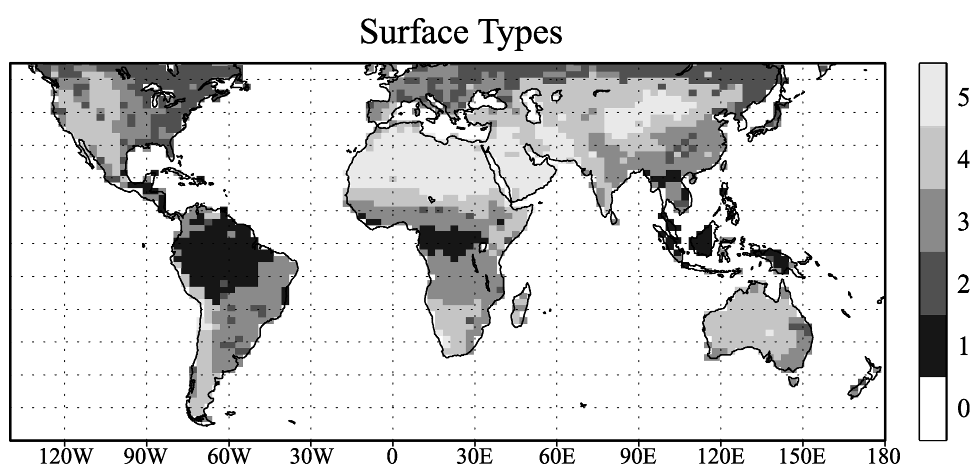

FIG. 1. Surface types prescribed in QTCM used to define roughness length and specify experimental regions. Based on vegetation classification of DeFries and Townshend (1994), 1: rainforest; 2: other forest; 3: moderate vegetation; 4: low vegetation; 5: desert; 0: water.

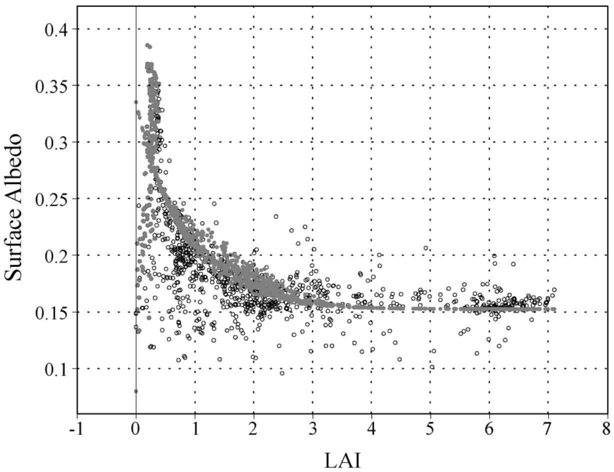

FIG. 2. Annual average observed LAI (ISLSCP, initiative 2) vs observed surface albedo (ERBE: black, open circles) and reconstructed albedo (gray dots) from Eq. (5).

of the five vegetation class regions to obtain a representative value. The roughness length is assumed not to depend on LAI.

3. Parameterization of surface albedo and surface conductance

a. Leaf area index data

Data for LAI (defined as the ratio of one-sided leaf area per land surface area) are from ISLSCP Initiative 2, based on observed Normalized Difference Vegetation Index (NDVI; Los et al. 2000; Sellers et al. 1994; Sellers et al. 1996b). These estimates of observed total LAI are used in the parameterization of land surface properties. Data covering the years from 1982 to 1990 were used and the LAI climatology is defined over this period.

b. Albedo parameterized on leaf area index

Land surface albedo, A_s, has been shown to depend on many properties including solar zenith angle, background soil type and moisture content, amount of green leaves, amount of dead leaves, leaf angle, and snow properties (Dickinson 1983; Sellers et al. 1996a,b). For the purposes of our simplified experiments we consider only leaf area index dependence in our A_s parameterization for most regions. Figure 2 shows the relationship between observed total LAI and observed land surface albedo using annual average values of LAI and albedo for 30°S–30°N. The land albedo product is from the Earth Radiation Budget Experiment (ERBE; Barkstrom et al. 1990). Our results were also checked with the Darnell et al. (1992) albedo product and were generally the same. The ISLSCP snow-free surface albedo was also evaluated and showed significant differences from the other two albedo products and so is not used here. Overall, A_s tends to decrease with increasing vegetation amount due to the high absorption of wavelengths in the region of photosynthetically active radiation (PAR) by plants. We use this general relationship to parameterize A_s; more complex behavior (see e.g., Wright et al. 1996) is modeled in other land surface schemes. For example, SiB2 (Sellers et al. 1996b) assumes brighter tropical forest canopies than tropical soils, so SiB2 albedo increases slightly with LAI in certain regions (a feature that does not appear in the data of Fig. 2).

To construct a simple parameterization of land surface albedo, we fit the data of Fig. 2 using the form

$$A_s = a - b(1 - e^{-ck\Lambda}), \tag{5}$$

where A_s is land surface albedo and Λ is LAI. The resulting parameterized albedo is also shown in Fig. 2 for $a = 0.3352$, $b = 0.1827$, and $c = 1.733$ with k, the extinction coefficient for photosynthetically active radiation, taken to be 0.75. The values of reconstructed albedo shown in Fig. 2 are annual average values based on the monthly climatology of observed LAI.

Soil reflectances with the exception of regions with very low leaf area index are neglected. Regions of vegetation class desert with climatological leaf area index less than 0.48 for at least 11 out of 12 months are sufficiently bare that leaf area index is not a good indicator of surface albedo. For these ''bare ground'' regions monthly climatological ERBE albedo (Barkstrom et al. 1990) is used in place of the parameterized albedo. Surface albedo for seasonally snow- or ice-covered regions is also prescribed by the observed value of ERBE albedo. As a proxy for snow cover, we consider monthly climatological albedo over 0.3 to indicate snow or ice cover for latitudes above 38°N. Missing values of the ERBE monthly climatological albedo are filled in with smoothed-ERBE monthly climatological albedo. Ocean albedo is set to a constant 0.08.

The annual average of the reconstructed albedo product is shown in Fig. 3. The general features of observed albedo are satisfactorily reproduced although differences for particular locations may be noted. In the model runs we use a 12-month climatology interpolated to the model calendar day.

c. Surface conductance parameterized on leaf area index

Plant roots and stomates along with the soil surface provide resistance to the movement of moisture from the surface to the atmosphere. Typically this surface resistance is characterized in land surface models by versions of the Penman–Monteith equation. We take a further simplified approach and parameterize a combined stomatal and root resistance that, together with aerodynamic resistance, modifies evaporation according to (3).

Our surface conductance parameterization uses a leaf to canopy scaling similar to Sellers et al. (1996a,b) and Zeng et al. (1999): g_s depends on leaf area index as

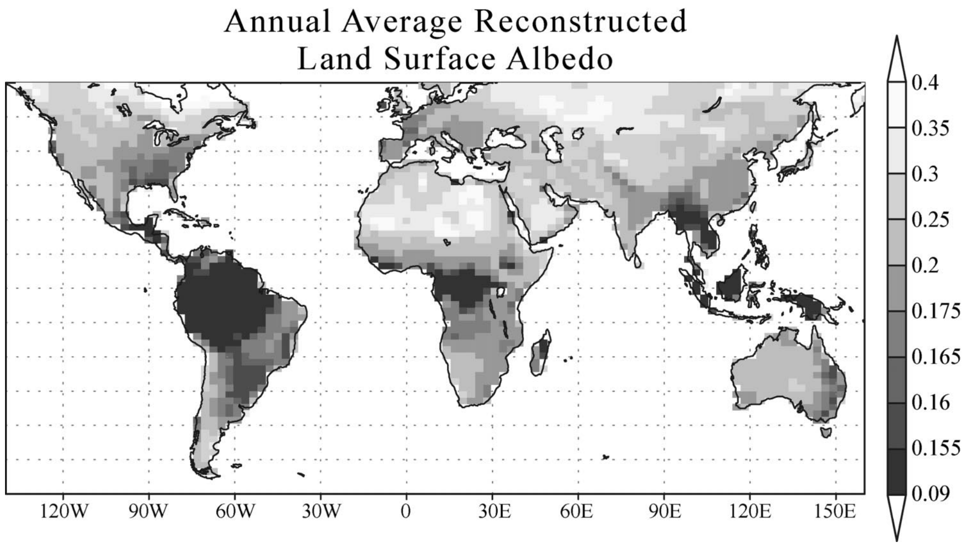

FIG. 3. Annual average reconstructed albedo from the parameterization given by Eq. (5) with observed climatological LAI.

$$g_s = g_{s_{\max}}\beta(w)(1 - e^{-k\Lambda})/k, \tag{6}$$

where $k = 0.75$ is the extinction coefficient, $\beta(w)$ is the soil moisture dependence ($\beta(w) = w^{1/4}$; w is wetness, ratio of soil moisture to field capacity), and $g_{s_{\max}}$ is 6.67 mm s^{-1} for tropical rainforest, and 5 mm s^{-1} for all other vegetation classes. Similar to other land surface schemes (e.g., BATS; Dickinson et al. 1993), we include a dependence on vegetation class in the minimum resistance to address differences in vegetation structure. Thus evaporation is modified by the total conductance of $1/(r_s + r_a)$, where r_a is aerodynamic resistance and r_s is surface resistance (inverse of surface conductance).

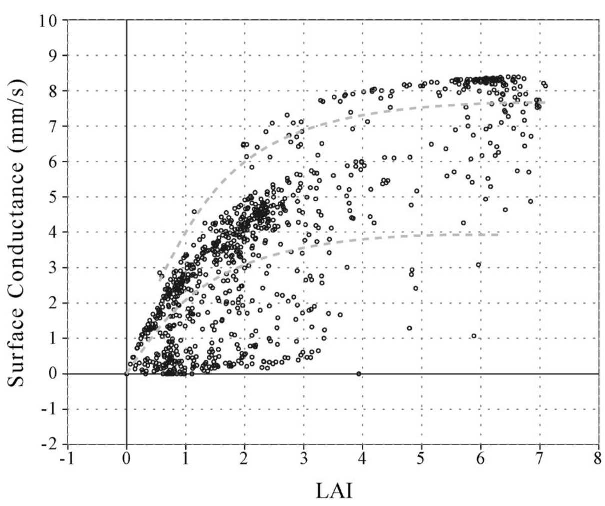

FIG. 4. Parameterized surface conductance, g_s, from Eq. (6) (open circles) vs annual average observed LAI including effects of modeled soil wetness. Upper gray dashed line shows g_s for rain forest regions using a value of soil wetness averaged over all rain forest and $g_{s_{\max}}$ = 6.67 mm s^{-1}. Lower gray dashed line shows g_s for other vegetation types (excluding desert/bare ground) with corresponding average soil wetness and $g_{s_{\max}}$ = 5 mm s^{-1}.

Resistance to evaporation between the soil surface and the atmosphere is not included explicitly in our formulation. For leaf area index less than 3, conductance is less than it would be if soil conductance were included. Our parameterization of g_s yields a relation to LAI similar to those discussed by Kelliher et al. (1995) and Schulze et al. (1994) for moderate to high LAI. Considering observations of stomatal conductance and canopy conductance and the predicted surface/canopy conductance of Schultze et al. (1994) the behavior of g_s in our model is reasonable with the caveat that our moderate vegetation class contains plants of many different types, including both agricultural and natural vegetation, and observed values of surface conductance vary greatly for this range of vegetation.

Figure 4 shows annually averaged leaf area index versus reconstructed surface conductance. Soil moisture dependence is included and contributes significantly to the scatter. For reference, values of g_s are also shown using annually and area-averaged values of soil wetness for rain forest (upper curve) and other vegetation types (lower curve, excluding desert/bare ground). Within the range of LAI typical of a given vegetation class, the impact of LAI on surface conductance is modest compared to the annual cycle of soil moisture, but can still be significant. In a fully interactive vegetation model where LAI is predicted according to soil moisture, LAI would depend on the past history of soil moisture, so would remain an independent physical effect.

4. Experimental design

a. Motivation and setup

To understand the sensitivity of the atmospheric response to changes in vegetation properties, LAI is al-

TABLE 2. Summary of sensitivity experiments: For each of the experiments listed, three cases are run: 1) LAI changed in both surface albedo and conductance, 2) LAI changed in A_s only, and 3) LAI changed in g_s only. For the vegetation class experiments, classes considered are rain forest, moderate vegetation, and low vegetation. Fine resolution is 2.8125° by 1.875° with a grid of 128 by 64. Coarse resolution is 5.625° by 3.75° with a grid of 64 by 32.

Vegetation sensitivity experiments		
Experiment region	Resolution	LAI change
Global vegetation	Coarse	−15% and +15%
Tropical vegetation class	Coarse	−33%
Regional vegetation class	Coarse	−33%
	Fine	−33% and −15%

tered over selected regions and 10 ensemble runs of 10 years each are conducted to produce 100 years of model output per experiment. Corresponding experiments are done with LAI impacts retained only in surface conductance (g_s only) and only in surface albedo (A_s only). Sea surface temperature is fixed to a 12-month climatology.

Examination of the 9-yr LAI record used here shows interannual variations of rainy season LAI between 13.5% and 47% of the mean averaged over our experimental regions. Arid regions tend to have larger interannual variations than forest regions. Variations in low vegetation regions are approximately 47%, moderate vegetation regions show typical variations of 19%, and rain forest regions show the least variation at around 14%. We choose two magnitudes of percent change in LAI: 15% change in LAI represents a perturbation to vegetation cover on the order of observed interannual changes in LAI in rain forest and moderate vegetation regions and 33% change represents a conservative interannual change in low vegetation regions. For consistency, each set of experiments has the same percent change in LAI. This experimental design may also be taken as representative of anthropogenic perturbations to vegetation cover through activities such as selective logging, grazing, and wood-fuel harvesting (e.g., Laurance et al. 2001; Ramankutty and Foley 1999), although we note the caveat that actual anthropogenic perturbations are more complex than the simple changes applied here.

b. *Summary of experiments*

Table 2 summarizes the various experiments to be analyzed. Our ‘‘Global’’ experiment changes LAI by 15% over all land surfaces. We also perturb LAI by a larger percentage, 33%, within given vegetation classes and constrain the perturbations to the Tropics (35°S–35°N). We term this set of experiments ‘‘Tropical Vegetation Class.’’ The LAI is perturbed in each vegetation class in turn (rain forest, moderate, and low vegetation). In assigning the regions for which LAI is perturbed, isolated points of a different vegetation class are also perturbed if sufficiently surrounded by the perturbed class for geographic cohesiveness. Finally, in our most specific experiments we use both coarse (64 × 32 grid boxes) and fine (128 × 64 grid boxes) spatial resolutions and focus on particular regions, namely equatorial and northern Africa, perturbing LAI by 33% in the coarse resolution and by 33% and 15% in the fine resolution over small regions of vegetation class. These experiments are termed ‘‘Regional Vegetation Class.’’ In each set of experiments (Global, Tropical, or Regional) the LAI perturbation takes three forms: LAI altered in both A_s and g_s, in A_s only, and in g_s only. We examine the fine-resolution, low LAI perturbation experiments for consistency with the more drastic experiments, keeping in mind that the variance in precipitation for these experiments is on the order of the sensitivity. This is due to higher model variance with fine resolution and smaller magnitude of sensitivity to smaller LAI perturbation.

5. Results and analysis

a. *Overall sensitivity to altered vegetation amount*

We first examine our most general set of experiments, ‘‘Global vegetation’’ with LAI changed by 15%. Precipitation anomalies for summer and winter seasons are shown in Fig. 5 for the reduced LAI case. Each of these experiments are 100-yr ensembles. Precipitation, evaporation, and surface temperature anomalies are contoured; shading indicates where the anomalies pass the 98% significance level for a Student’s t test for two distributions. In the case of precipitation, regions of climatological precipitation less than 2 mm month^{-1} are not shaded (for all figures) since the condition of normality of the distributions of anomalies required for the Student’s t test may hold less well.

Precipitation anomalies in both June–July–August (JJA) and December–January–February (DJF) reach a magnitude of more than 10 mm month^{-1} over areas of Africa. Over the Amazon they exceed 8 mm month^{-1} in DJF (4 mm month^{-1} in JJA). This is a modest perturbation compared to the climatology in the rain forest region and is a more significant perturbation in savanna regions of Africa. The model’s climatological precipitation is spread over a slightly larger latitude band than is seen in observations in Africa [Xie and Arkin 1997; see Zeng et al. (2000) for QTCM climatology and a later version in Lin and Neelin (2002), their Fig. 7]. This may affect the latitude extent of the anomalies in this region. In DJF, precipitation anomalies in South America are larger due to the presence of the summer monsoon convection. Part of the pattern along the southern edge of the South American convergence zone does not pass 98% significance due to the considerable natural variability there.

Evaporation anomalies (E') (Figs. 5c and 5d) are smaller than precipitation anomalies (P') over land re-

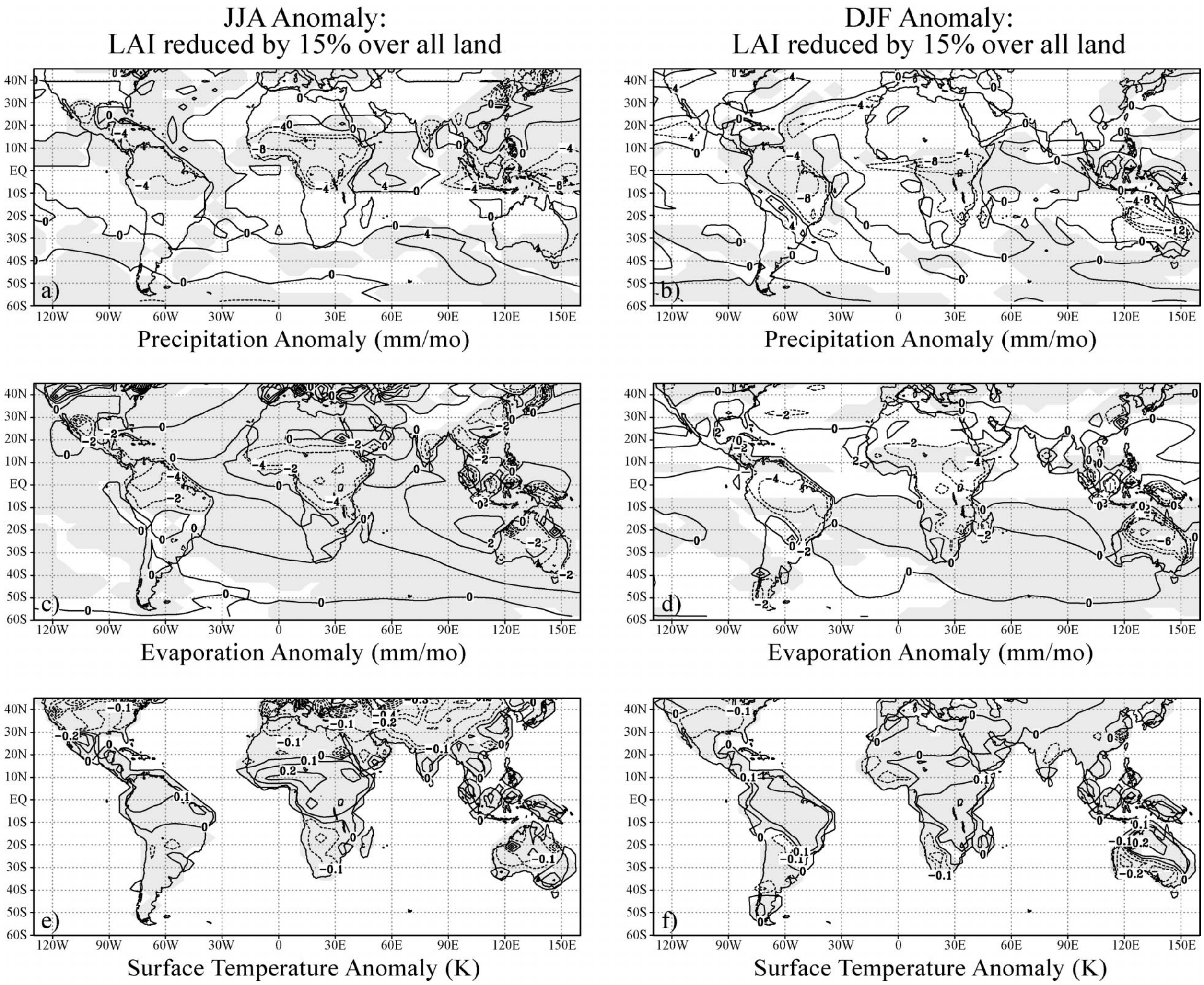

FIG. 5. Global land experiment with LAI reduced by 15% in both A_s and g_s minus the control experiment (a), (b) P'; (c), (d) E'; and (e), (f) T_s' for JJA and DJF, respectively. Precipitation contour interval 4 mm month^{-1} and evaporation contour interval 2 mm month^{-1}. Surface temperature contour interval 0.1 K. Shading in all panels indicates 98% significance for 100-yr average anomalies of the given variable and season.

gions, suggesting that convergence feedback in the atmosphere is involved in at least some places. Evaporation anomalies are comparable to P' over the Amazon and approximately half the P' over much of Africa. Figures 5e and 5f show modest surface temperature anomalies (T_s') reaching only a few tenths of a degree Celsius, but the statistical significance of the anomalies allows us to analyze mechanisms associated with them.

Overall, with LAI decreased by 15%, altering both surface albedo and conductance, we see decreased precipitation, decreased evaporation, and increased surface temperature. This is consistent with the July tropical results of Bounoua et al. (2000) in which GCM model runs were compared with maximum observed NDVI versus minimum observed NDVI (grid boxwise). One difference is that in Bounoua et al. precipitation changes are smaller than evaporation changes. This is likely related to their albedo parameterization, which tends to have increasing albedo with increasing NDVI in certain tropical regions (to represent dark tropical soils). Further, their averages over 14.4°S to 14.4°N leave out some moderate and low vegetation regions such as the Sahel.

In order to summarize a large number of experiments, Table 3 shows JJA precipitation, evaporation, surface temperature, and albedo anomalies in the local impact zone of each experiment. We define the ''local impact zone'' for each experiment as the region in the LAI case that is local to the perturbed LAI and has JJA P' of 4 mm month^{-1} or more for experiments with LAI reduced by 33% and 2 mm month^{-1} or more for experiments with LAI reduced by 15% with a minimum significance level of 98%. The regions of P' impact tend to be larger than the regions of local LAI change, thus some significant nonlocal anomalies are excluded in the sum-

TABLE 3. Seasonal JJA local impact zone anomalies: Leaf area index is altered in 1) both A_s and g_s for the ''LAI'' experiments, 2) only in A_s for the A_s-only experiments, and 3) only in g_s for the g_s-only experiments. Impact zones are defined by the area with a minimum P' of 4 (for LAI −33%) or 2 (for LAI −15%) mm month^{-1} in the region of local LAI perturbation and that satisfies the 98% confidence level for the given experiments' LAI case precipitation anomaly. The impact zone from the LAI case is used for the associated A_s-only and g_s-only experiments. NS denotes not statistically significant.

Experiment		P' (mm month^{-1})	E' (mm month^{-1})	T'_s (K)	ΔA_s
		Coarse resolution, LAI−15%			
Global vegetation	LAI	−7.4	−4.3	0.14	0.00478
	A_s only	−5.1	−1.0	NS	0.00478
	g_s only	−2.5	−3.5	0.14	0
		Coarse resolution, LAI+15%			
Global vegetation	LAI	6.2	3.9	−0.13	−0.00373
	A_s only	3.8	0.7	NS	−0.00373
	g_s only	2.9	3.1	−0.13	0
		Coarse resolution, LAI−33%			
Tropical rain forest	LAI	−10.9	−10.3	0.26	0.00511
	A_s only	−3.0	−0.5	−0.01	0.00511
	g_s only	−7.8	−9.9	0.27	0
Tropical moderate vegetation	LAI	−16.0	−10.3	0.40	0.0149
	A_s only	−9.4	−1.7	−0.05	0.0149
	g_s only	−5.7	−8.6	0.46	0
Tropical low vegetation	LAI	−16.4	−9.6	0.33	0.0181
	A_s only	−10.9	−2.0	−0.10	0.0181
	g_s only	−6.5	−8.1	0.46	0
		Coarse resolution, LAI−33%			
Africa rain forest	LAI	−12.5	−12.5	0.36	0.00447
	A_s only	−3.2	−0.4	NA	0.00447
	g_s only	−9.6	−12.1	0.37	0
North Africa moderate vegetation	LAI	−14.2	−11.2	0.45	0.0154
	A_s only	−7.5	−1.7	−0.04	0.0154
	g_s only	−6.9	−9.6	0.50	0
North Africa low vegetation	LAI	−16.2	−9.7	0.34	0.0187
	A_s only	−10.5	−1.8	−0.11	0.0187
	g_s only	−6.8	−8.3	0.48	0
		Fine resolution, LAI−33%			
Africa rain forest	LAI	−9.0	−11.6	0.33	0.00289
N. Africa moderate vegetation	LAI	−12.6	−10.5	0.43	0.0132
N. Africa low vegetation	LAI	−13.9	−10.0	0.34	0.0194
		Fine resolution, LAI−15%			
Africa rain forest	LAI	−3.0	−5.3	0.15	0.00040
	A_s only	NS	NS	−0.01	0.00040
	g_s only	−3.6	−5.3	0.16	0
N. Africa moderate vegetation	LAI	−4.5	−4.2	0.18	0.00460
	A_s only	−2.3	−0.6	−0.01	0.00460
	g_s only	−2.2	−3.6	0.18	0
N. Africa low vegetation	LAI	−5.8	−4.2	0.14	0.00792
	A_s only	−3.2	−0.7	−0.05	0.00792
	g_s only	−1.6	−3.5	0.20	0

marized results (for a discussion of the nonlocal anomalies, see section 5c). The local impact zone defined for the LAI case is used for the corresponding g_s-only and A_s-only experiments.

The first entry of Table 3 is the Global LAI case, discussed above. Also included are the anomalies for the Global experiment with only albedo changed and only surface conductance changed. The individual A_s-only and g_s-only experiments show that both parameters contribute significantly to the atmospheric response. The A_s-only experiment produces a larger response in P' (−5.09 versus −2.51 mm month^{-1}), while the g_s-only experiment produces a larger response in both E' (−3.49 versus −1.01 mm month^{-1}) and T'_s (0.14 versus 0.01 K), Table 3. For the Global LAI case with LAI increased by 15%, anomalies are similar to the decreased LAI 15% case (Table 3) but with opposite sign and slightly smaller magnitude. This case tends to be similar regionally (figure not shown) to Fig. 5 with the exception of smaller precipitation anomalies over the Amazon. The partitioning between A_s and g_s is consistent between the −15% and +15% Global LAI cases (Table 3) with a slightly weaker A_s contribution in the LAI +15% case. The other experiments listed in Table 3 aim to understand the relative importance of these two parameters in land–atmosphere interactions.

b. Relative influence of surface conductance and albedo for different vegetation types

To compare the relative influence of surface albedo and surface conductance in different regions, LAI is modified in one land surface vegetation class at a time as described in section 4b. We note that the vegetation classes are used to organize the regions but that LAI varies continuously and that sensitivity will depend on background climate factors such as precipitation and soil moisture. In Table 3, Tropical Vegetation Class experiment results are reported for all local impact zones. In Fig. 6 we highlight the impacts on precipitation seen on the South American and African continents since these are the regions of the most interesting results as well as where our model is most trustworthy. We avoid focus on Australia as this QTCM version produces an Australian monsoon that extends too far south in DJF.

The vegetation class regions on the finer of the two resolutions used in experiments in this study are shown in Fig. 1. For the coarse-resolution experiments discussed in this section, some finer-scale features are lost but generally the two maps look quite similar. The top row of Fig. 6 shows the regions of perturbed LAI for Africa and South America for each of the three sets of experiments discussed in this section.

Table 3 and Fig. 6 show that the impact from a given *fractional* change in LAI on overall precipitation, evaporation, or surface temperature in the impact zone is comparable for the three vegetation class experiments even though the actual value of the LAI change is very different. A 33% decrease is equivalent to reducing the average JJA value of LAI by 1.45 in the rain forest, 0.696 in moderate vegetation regions, but only 0.384 in low vegetation regions. This provides some justification for the use of percent change experiments rather than a fixed LAI decrease.

The anomalies from the A_s-only and g_s-only experiments (Table 3 and Fig. 6) roughly combine to the anomaly of the LAI experiment. For example, when A_s and g_s are altered independently, the tropical moderate vegetation class experiment has a P' of -9.36 and -5.86 mm month^{-1}, respectively. These anomalies roughly add up to the P' value of -16.01 mm month^{-1} when both are altered in the combined experiment. We can thus use the independent A_s and g_s experiments to analyze mechanisms in the LAI experiment.

For the tropical rain forest experiment, neither A_s or g_s is negligible, but g_s is responsible for approximately 2/3 of the precipitation response (Table 3). The tropical moderate vegetation experiment, in contrast to the rain forest case, has a stronger response to the change in A_s, accounting for about 60% of the combined precipitation anomaly. For the tropical low-vegetation experiment, changes in A_s have a larger influence than changes in g_s contributing close to 2/3 of the LAI precipitation response. This difference in the impacts of A_s and g_s between vegetation class experiments also holds region by region in the plots of Fig. 6. Note that since Fig. 6 shows JJA anomalies, little effect is seen in South America for the moderate vegetation region.

The LAI dependence of both g_s and A_s is such that there is a smaller change in their values for a given change in LAI at higher LAI than at lower (Figs. 2 and 4). Thus, in the albedo experiments we are altering albedo more in the less vegetated experimental regions than in the more heavily vegetated regions. For g_s, though its dependence on LAI is also saturated at high LAI, more arid regions have less water available for evapotranspiration. Thus, although g_s is more sensitive at low LAI, we see the greatest influence from g_s changes at high LAI since the contribution from evapotranspiration to total evaporation and precipitation is largest there.

There are also other differences in the mechanisms by which g_s and A_s affect P'. Changes to surface conductance directly alter evapotranspiration. Evaporation anomalies tend to be similar or larger than precipitation anomalies for g_s experiments (mostly from changing the recycling of water and losing some to moisture divergence). Consistent with this, the LAI rain forest experiment response is dominated by g_s effects with P' and E' of similar magnitude (Table 3) while moderate and low vegetation tend to be dominated by A_s with larger P' than E'. Interestingly in Figs. 6f,i,l, g_s impacts on precipitation appear more local than the A_s impacts (likely due to the fact that g_s changes do not alter total energy balance of the atmospheric column above the perturbed LAI). An albedo perturbation directly changes the energy available to the atmospheric column (Charney et al. 1977; Zeng and Neelin 1999). For an increase in surface albedo, less solar radiation is absorbed thereby decreasing total net energy of the column. This direct thermodynamic effect changes the energy available for convection, reducing the chance for precipitation and rising motion. Additionally, cooler atmospheric temperatures can be exported nonlocally by wave dynamics. For the albedo case, the evaporation response is much smaller than the precipitation response (due to moisture convergence) in each of the Tropical Vegetation Class A_s-only experiments.

To summarize, the relative influence of surface conductance and albedo depends on vegetation class and the associated background climate. In the rain forest surface-type experiment, changes to surface conductance produce larger anomalies than a similar change in albedo. For the low-vegetation surface-type experiment, we see a larger influence from changes in surface albedo than from changes in surface conductance in these arid regions.

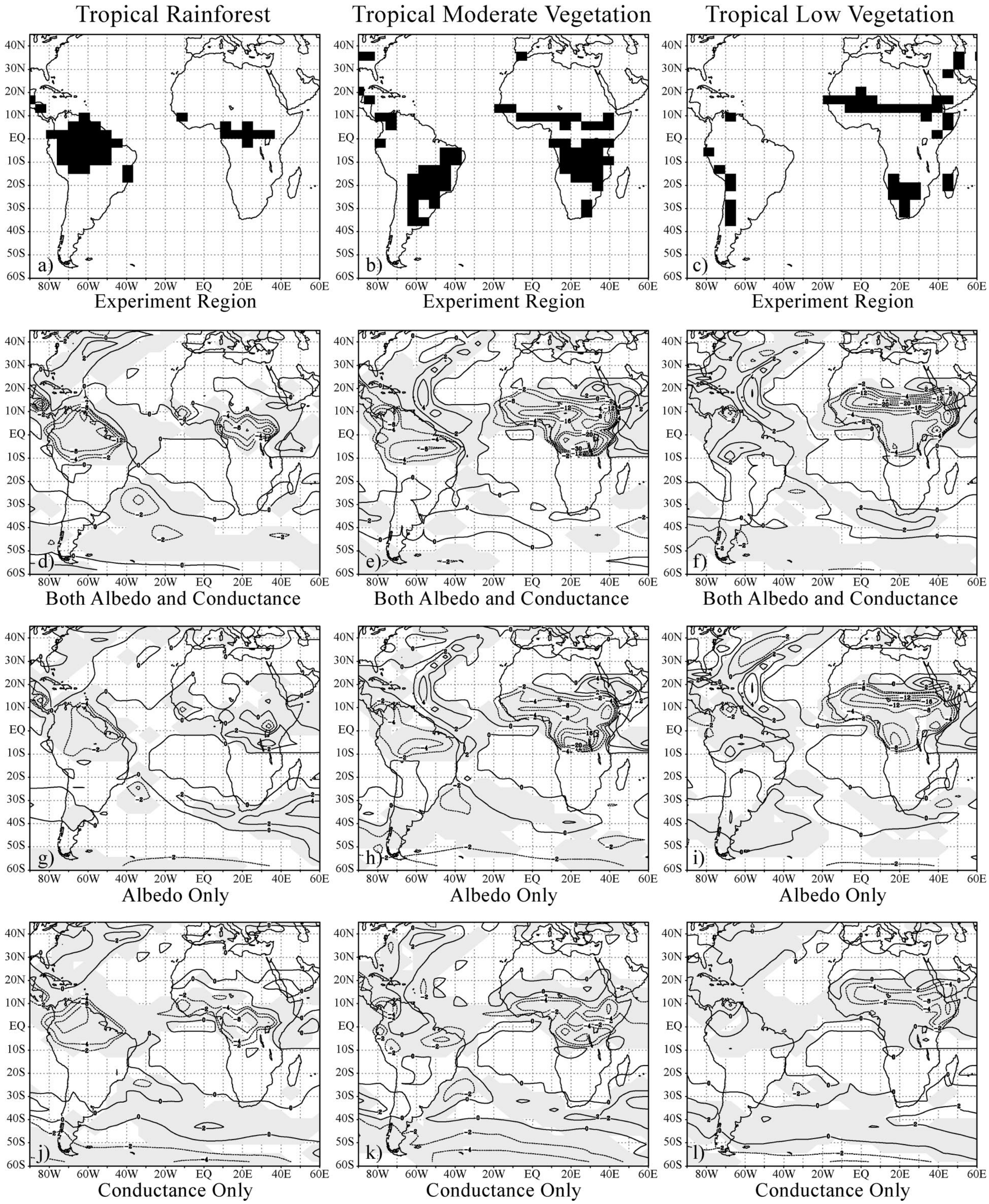

FIG. 6. JJA precipitation anomalies (mm month^{-1}) for the tropical experiments with LAI reduced by 33%. (a)–(c) Experimental regions. LAI reduced by 33% in (d)–(f) both A_s and g_s, in (g)–(i) A_s only, and in (j)–(l) g_s only for (left column) tropical rain forest, (middle column) tropical moderate vegetation, and (right column) tropical low vegetation. Shading indicates 98% significance in the difference between the LAI case and (d)–(f) the control run and 98% significance in the difference between the LAI case and the (g)–(l) A_s-only and g_s-only cases. Contours at 4 mm month^{-1}.

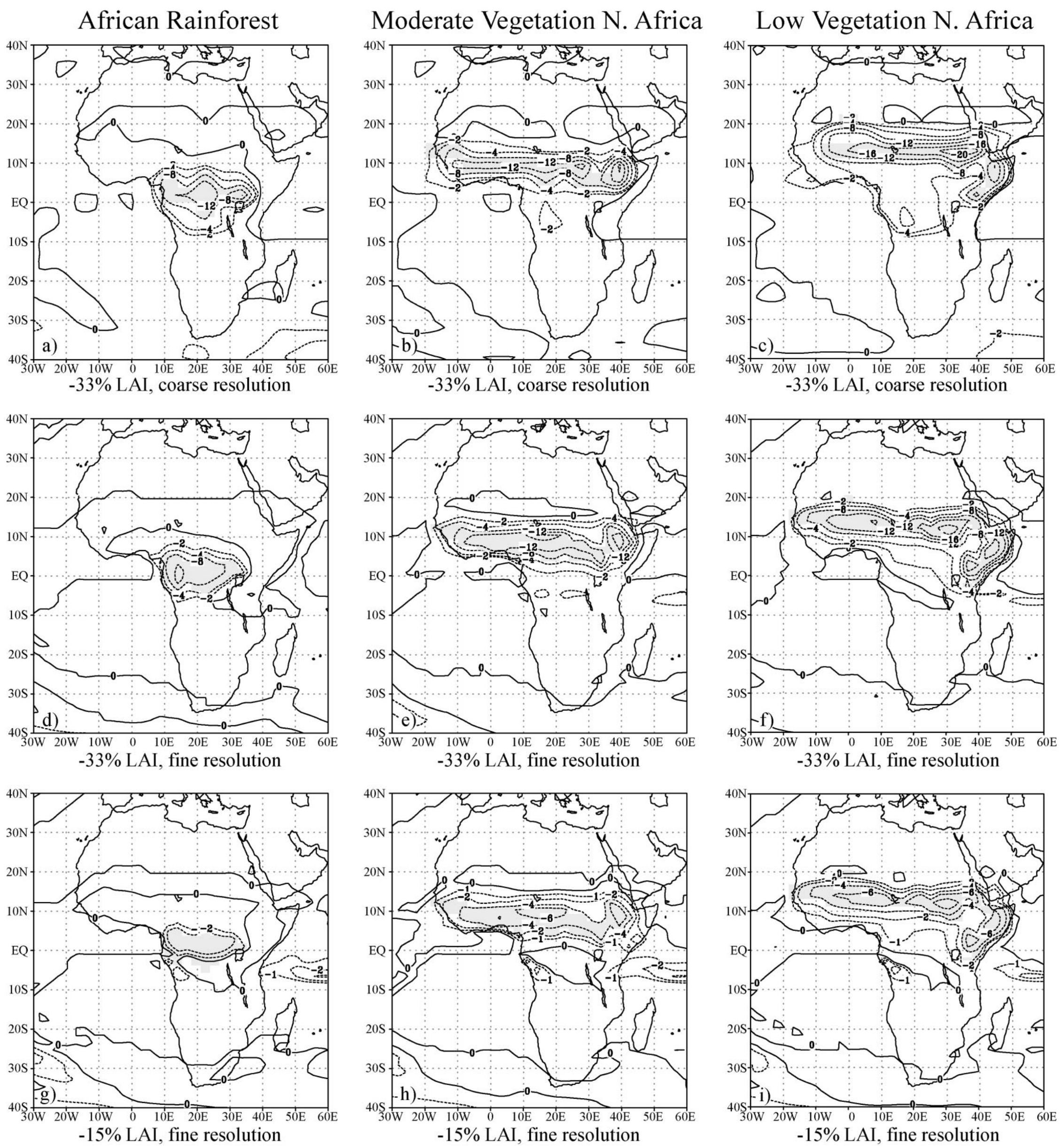

FIG. 7. JJA precipitation anomalies (mm month^{-1}) for the African Regional experiments, for (a)–(c) LAI −33%, coarse resolution, (d)–(f) LAI −33%, fine resolution; and (g)–(i) LAI −15%, fine resolution in (left column) African rain forest case, (middle column) North African moderate vegetation case, and (right column) North African low vegetation case. Shading indicates regions of perturbed LAI.

c. *Sensitivity of local and nonlocal effects*

Fine-resolution LAI perturbation experiments generally show similar results to the coarse-resolution experiments. There appears, however, to be a tendency to produce nonlocal precipitation anomalies in the coarse resolution of the model that are not seen in the fine-resolution runs, especially in the low vegetation case. To examine this behavior, we look at the African Regional experiments with coarse resolution and LAI −33% (Figs. 7a,b,c), fine resolution and LAI −33% (Figs. 7d,e,f), and fine resolution with LAI −15% (Figs. 7g,h,i). The zones of perturbed LAI are shown as shaded grid boxes in Fig. 7.

The African rain forest experiments produce anomalies that are consistently local to the altered regions for the two resolutions and LAI perturbations (Figs. 7a,d,g). In this case, the precipitation response is more than 3 times larger in the LAI −33% case than in the −15% case. Since both g_s and A_s are saturated at high LAI, the larger change in LAI produces a much larger change in these parameters. The last column of Table 3 shows the change in A_s in the impact zone for each experiment. An LAI change of −15% corresponds to an albedo change of only 0.0004 versus the albedo change for LAI −33% of 0.0029, more than 7 times larger. The fine-resolution, LAI −15%, African rain forest experiment reveals smaller-scale features of the response, as can be seen in the slight positive anomaly to the south of the experiment region. Its location is consistent with increased precipitation along the southern edge of the convective region.

The moderate vegetation, North Africa, case (Fig. 7e) is very similar to the tropical moderate vegetation case (Fig. 6e) in the regions local to the North African LAI change. In Fig. 6e, anomalies in the equatorial African region between the regions of LAI change show the influence of remote effects on the precipitation. The nonlocal precipitation anomalies in the moderate vegetation cases in Figs. 7b,e,h are smaller in magnitude since only the North African region LAI is changed. The small nonlocal anomalies south of the perturbed region are statistically significant in the LAI −33% cases (the positive anomaly in the −15% LAI case does not pass at the 98% significance level). In coarse- and fine-resolution LAI −33% experiments small nonlocal negative anomalies occur around 5°S (Figs. 7b,e), so this effect appears relatively insensitive to resolution.

The largest nonlocal precipitation anomaly appears in the coarse-resolution, low vegetation North Africa, LAI −33% case. This nonlocal anomaly located south of the experiment region is approximately 1/3 of the typical maximum anomaly in the local region (Fig. 7c). In the fine-resolution case, it is less than 1/6 for both the −33% and −15% LAI cases (Figs. 7f,i). Thus for this case, the nonlocal effects do appear sensitive to resolution.

Between the two resolutions of the LAI −33% case there are also differences in the magnitude of P'. Each of the vegetation region experiments have slightly larger P' (by roughly 15% for averages in Table 3) in the coarse resolution than in the fine resolution. This may be due to the slight differences in the areas assigned to each region on the different grids.

In the low vegetation, North Africa case the percentage contributions from A_s-only and g_s-only experiments to P' are larger from the A_s case, consistent with the tropical low vegetation experiment results. The LAI −15%, fine-resolution case has an A_s response almost twice the g_s response in precipitation, a contribution even larger than in the tropical low vegetation case. Here P' from A_s-only and g_s-only experiments in the North African, moderate vegetation case with both −33% and −15% LAI are quite similar in their relative contributions from A_s and g_s to precipitation. Generally, A_s has a larger influence in all moderate vegetation experiments. For the North African experiments the P' from the A_s-only experiment is only 6%–8% larger than that from the g_s-only experiments while in the tropical moderate vegetation, LAI −33% case, it is approximately 60% larger. In the African rain forest, LAI −33% case, A_s and g_s relative contributions are very similar to the tropical rain forest LAI −33% case. Both show g_s contributing over 60% more than the A_s contribution. In the African rain forest, LAI −15%, A_s-only case, P' is not statistically different from zero.

Overall, comparing the coarse-resolution (Fig. 7) with the fine-resolution experiments for differing LAI perturbations (Fig. 7), the local signal is generally robust including the relative roles of albedo and surface conductance for the three vegetation classes. The remote signals are substantially smaller than the local signals, and the robustness appears to vary among experiments.

d. Competing mechanisms producing surface temperature anomalies

From general inspection of our experiments, we see that a decrease in LAI corresponds to a decrease in precipitation and an increase in surface temperature. This is consistent with the relationships found by Los et al. (2001) who examined statistical correlations between 9-yr records of vegetation (NDVI), precipitation, and land surface air temperature.

However we expect competing mechanisms to affect surface temperature. The direct thermodynamic effect of increased surface albedo decreasing absorbed solar radiation should reduce surface temperature. Decreased surface conductance is expected to reduce evaporation in the experiment zone allowing less latent heat to leave the surface, which should then be balanced by an increase in surface temperature.

Figure 8 shows surface temperature anomalies for the African-Regional low vegetation experiment (coarse resolution, LAI −33%). Surface temperature anomalies in this experiment are positive in the local region of the LAI anomaly (Fig. 8a). This is also seen in the experiment in which g_s is altered while A_s remains at the control value (Fig. 8c). However, the A_s-only experiment produces a negative surface temperature anomaly (Fig. 8b).

We choose the African-Regional, low vegetation, LAI −15% experiment to illustrate the effect; however, this pattern is seen in all of our tropical and African sensitivity experiments. Table 3 shows this tendency in the local impact zones. The negative T_s anomaly in the A_s-only case is generally local to the experiment region and is considerably smaller in magnitude than the positive anomalies seen in the LAI and g_s-only cases (Fig. 8 and Table 3). Within the Tropics the effect on surface temperature is dominated by the influence of surface conductance as seen by comparison of the LAI experiments and A_s-only and g_s-only experiments. In the moderate vegetation and rain forest cases, the A_s effect on T_s is about an order of magnitude weaker than in the low vegetation case due to the saturated behavior of albedo for higher LAI values. For the Global case, we see similar dominance of g_s in the Tropics (figure not

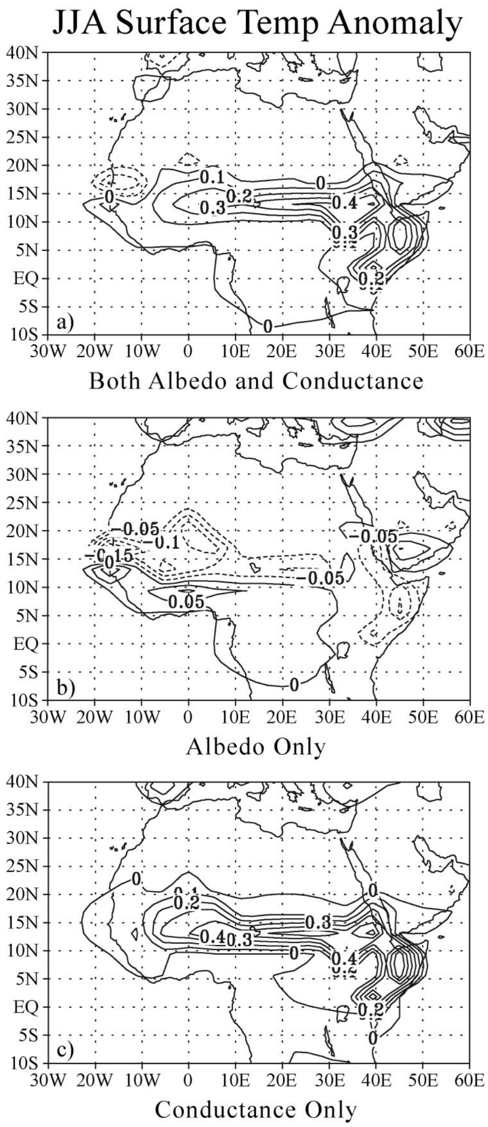

FIG. 8. JJA surface temperature anomalies for (a) both, (b) A_s-only, (c) g_s-only, low-vegetation, North African regional, LAI −33% experiments.

shown). The dominance of g_s does not hold outside of the Tropics, however, where A_s impacts are of the same magnitude or larger and the g_s impacts are of smaller amplitude and display more complex seasonal dependence.

6. Conclusions

With the QTCM's intermediate-complexity model physics and simple land surface scheme we see sensitivities to changes in land surface albedo and surface conductance consistent with previous studies (Bounoua et al. 2000; Xue and Shukla 1993; Hahmann and Dickinson 1997; Dirmeyer and Shukla 1994; Cox et al. 2000). Here we have placed both of these quantities on the same footing, that is, both are parameterized on LAI, so their impacts may be compared. We note the caveat that the exact percent contribution of surface albedo and surface conductance to the total anomaly depends on the parameterization used, and here the parameterizations are designed to capture the general behavior over the whole range of LAI rather than relationships within specific vegetation types. Our results should be viewed as a set of albedo change and surface conductance change experiments with the changes linked in a plausible way by the simple LAI parameterization. We also note that our experiments are organized with perturbations in different vegetation class regions but that the response will depend upon both the parameterized vegetation characteristics of the region and the background climatology (e.g., rain forests coincide with high climatological rainfall and soil wetness).

For experiments in which LAI changes of 15% and 33% are used, the responses in precipitation, evaporation, and surface temperature are modest though not negligible compared to interannual climate variability. Impacts arising from LAI perturbations are on the order of variability on slightly longer time scales and so are likely to be climatically important if they are sustained over a number of years. For instance, considering observed precipitation (Hulme 1992; Hulme et al. 1998) over regions similar to our North Africa perturbation areas, the standard deviation of 5-yr averages of JJA for 95 years of data range from approximately 17 mm month^{-1} for North African low vegetation to 14 mm month^{-1} for African rain forest. The standard deviation of yearly JJA averages is 30 mm month^{-1} and 33 mm month^{-1} for these regions. For LAI reduced by 33% in the coarse resolution, we see JJA precipitation decreased by 16 and 13 mm month^{-1} for the comparable regions, respectively.

Sensitivity in the Tropics to a given percent change in LAI in this model results in a higher precipitation anomaly in low and moderate vegetation regions than in rain forest regions. In terms of percent change from the climatology, this is a much larger sensitivity in low and moderate vegetation regions. The sensitivity to albedo change in semidesert regions has been noted in many past studies. Here we put this in perspective with the impacts due to surface conductance. Nonlocal effects seen in our coarse-resolution experiments are not found to the same extent in our fine-resolution experiments. Thus we focus on the robust local anomalies in all experiments. We note that long runs were used to establish statistical significance when displaying maps of the response to avoid the appearance of spurious remote anomalies.

By altering surface albedo and surface conductance separately, we compare their relative influence on the atmosphere. The anomalies produced in the individual experiments roughly add up to the combined change experiment, indicating fairly linear behavior of this decomposition. Albedo and surface conductance effects on surface temperature produce opposite tendencies, as expected, but surface conductance clearly dominates the combined sensitivity.

The impacts of changes in surface conductance and albedo on precipitation and evapotranspiration are of the same sign, but their relative importance differs among experiments with perturbations in different vegetation class regions. For all vegetation-type experiments neither effect is negligible. For comparable changes in surface albedo and surface conductance, more than half the sensitivity in precipitation over rain forests is due to the change in surface conductance. Over moderate vegetation, the influence of these two parameters is more similar, approximately 40% and 60% influence from surface conductance and surface albedo, respectively. Surface albedo has the most impact in low vegetation regions where it accounts for almost 70% of the combined precipitation anomaly. Overall, the larger influence of surface conductance in wetter, more heavily vegetated regions gives way to stronger influence of albedo in more arid, less vegetated regions.

The mechanism producing precipitation anomalies and the relation to evapotranspiration anomalies differs for albedo and surface conductance contributions and thus varies among differing climate regimes, here represented by vegetation class. Surface conductance changes create precipitation anomalies similar to evaporation anomalies (but of slightly smaller magnitude) driven by changes in the local recycling of water. Albedo changes alter the energy budget of the column and thus the moisture convergence, creating larger changes in precipitation than in evaporation.

Acknowledgments. This research was supported in part by National Science Foundation Grant ATM-0082529, National Oceanographic and Atmospheric Administration Grant NA 16GP2004, and National Aeronautics and Space Administration Grant NA G5-9358. The authors thank R. Koster for discussion and J. Meyerson for graphics assistance.

REFERENCES

Barkstrom, B. R., E. F. Harrison, and R. B. Lee, 1990: Earth Radiation Budget Experiment, Preliminary seasonal results. *Eos, Trans. Amer. Geophys. Union,* **71,** 297–304.

Bounoua, L., G. J. Collatz, S. O. Los, P. J. Sellers, D. A. Dazlich, C. J. Tucker, and D. A. Randall, 2000: Sensitivity of climate to changes in NDVI. *J. Climate,* **13,** 2277–2292.

Charney, J. G., 1975: Dynamics of deserts and droughts in Sahel. *Quart. J. Roy. Meteor. Soc.,* **101,** 193–202.

——, W. J. Quirk, S. H. Chow, and J. Kornfield, 1977: A comparative study of the effects of albedo change on drought in semi-arid regions. *J. Atmos. Sci.,* **34,** 1366–1385.

Cox, P. M., R. A. Betts, and C. D. Jones, 2000: The impact of dynamic vegetation on Sahelian climate variability in a GCM. *Eos, Trans. Amer. Geophys. Union,* **81** (Suppl.), Abstract B61D-02.

Darnell, W. L., W. F. Staylor, S. K. Gupta, N. A. Ritchey, and A. C. Wilber, 1992: Seasonal variation of surface radiation budget derived from International Satellite Cloud Climatology Project C1 data. *J. Geophys. Res.,* **97,** 15 741–15 760.

DeFries, R. S., and J. R. G. Townshend, 1994: NDVI-derived land cover classifications at a global scale. *Int. J. Remote Sens.,* **15,** 3567–3586.

Delire, C., P. Behling, M. T. Coe, J. A. Foley, R. Jacob, J. Kutzbacin, Z. Liu, and S. Yarrus, 2001: Simulated response of the atmosphere–ocean system to deforestation in the Indonesian Archipelago. *Geophys. Res. Lett.,* **28,** 2081–2084.

Dickinson, R. E., 1983: Land surface processes and climate–surface albedos and energy balance. *Advances in Geophysics,* Vol. 25. Academic Press, 305–353.

——, 1992: Changes in land use. *Climate System Modeling,* K. E. Trenberth, Ed., Cambridge University Press, 689–701.

——, and A. Henderson-Sellers, 1988: Modeling tropical deforestation: A study of GCM land-surface parameterizations. *Quart. J. Roy. Meteor. Soc.,* **114,** 439–462.

——, ——, and P. J. Kennedy, 1993: Biosphere–Atmosphere Transfer Scheme (BATS) Version 1e as coupled to the NCAR Community Climate Model. NCAR Tech. Note NCAR/TN-387+STR, Boulder, CO, 72 pp.

Dirmeyer, P. A., 1992: GCM studies of the influence of vegetation on the general circulation: The role of albedo in modulating climate change. Ph.D. thesis, University of Maryland, 227 pp.

——, and J. Shukla, 1994: Albedo as a modulator of climate response to tropical deforestation. *J. Geophys. Res.,* **99,** 20 863–20 877.

Dorman, J. L., and P. J. Sellers, 1989: A global climatology of albedo, roughness length and stomatal resistance for atmospheric general circulation models as represented by the Simple Biosphere Model (SiB). *J. Appl. Meteor.,* **28,** 833–855.

Entekhabi, D., and P. S. Eagleson, 1989: Land surface hydrology parameterization for atmospheric general circulation models including subgrid scale spatial variability. *J. Climate,* **2,** 816–832.

Hahmann, A. N., and R. E. Dickinson, 1997: RCCM2-BATS model over tropical South America: Applications to tropical deforestation. *J. Climate,* **10,** 1944–1964.

Henderson-Sellers, A., Z.-L. Yang, and R. E. Dickinson, 1993: The Project for Intercomparison of Land-surface Parameterization Schemes. *Bull. Amer. Meteor. Soc.,* **74,** 1335–1349.

Hulme, M., 1992: A 1951–80 global land precipitation climatology for the evaluation of general circulation models. *Climate Dyn.,* **7,** 57–72.

——, T. J. Osborn, and T. C. Johns, 1998: Precipitation sensitivity to global warming: Comparison of observations with HadCM2 simulations. *Geophys. Res. Lett.,* **25,** 3379–3382.

Kelliher, F. M., R. Leuning, M. R. Raupach, and E.-D. Schulze, 1995: Maximum conductances for evaporation from global vegetation types. *Agric. For. Meteor.,* **73,** 1–16.

Koster, R. D., and P. C. D. Milly, 1997: The interplay between transpiration and runoff formulations in land surface schemes used with atmospheric models. *J. Climate,* **10,** 1578–1591.

Laurance, W. F., M. A. Cochrane, S. Bergen, P. M. Fearnside, P. Delamonica, C. Barber, S. D'Angelo, and T. Fernandes, 2001: The future of the Brazilian Amazon. *Science,* **291,** 438–439.

Lean, J., and D. A. Warrilow, 1989: Simulation of the regional climatic impact of Amazon deforestation. *Nature,* **342,** 411–413.

Lin, J. W.-B., and J. D. Neelin, 2002: Considerations for stochastic convective parameterization. *J. Atmos. Sci.,* **59,** 959–975.

Lofgren, B. M., 1995a: Sensitivity of land–ocean circulations, precipitation, and soil moisture to perturbed land surface albedo. *J. Climate,* **8,** 2521–2542.

——, 1995b: Surface albedo–climate feedback simulated using two-way coupling. *J. Climate,* **8,** 2543–2562.

Los, S., and Coauthors, 2000: A global 9-yr biophysical land surface dataset from NOAA AVHRR data. *J. Hydrometeor.,* **1,** 183–199.

——, G. J. Collatz, L. Bounoua, P. J. Sellers, and C. J. Tucker, 2001: Global interannual variations in sea surface temperature and land surface vegetation air temperature, and precipitation. *J. Climate,* **14,** 1535–1549.

Neelin, J. D., and N. Zeng, 2000: A quasi-equilibrium tropical circulation model—Formulation. *J. Atmos. Sci.,* **57,** 1741–1766.

Ramankutty, N., and J. A. Foley, 1999: Estimating historical changes in global land cover: Croplands from 1700 to 1992. *Global Biogeochem. Cycles,* **13,** 997–1027.

Schulze, E.-D., F. M. Kelliher, C. Korner, J. Lloyd, and R. Leuning, 1994: Relationships among maximum stomatal conductance, ecosystem surface conductance, carbon assimilation rate, and plant nitrogen nutrition: A global ecology scaling excercise. *Annu. Rev. Ecol. Syst.,* **25,** 629–660.

Sellers, P. J., S. O. Los, C. J. Tucker, C. O. Justice, D. A. Dazlich, G. J. Collatz, and D. A. Randall, 1994: A global 1 by 1 degree NDVI data set for climate studies. Part 2: The generation of global fields of terrestrial biophysical parameters from the NDVI. *Int. J. Remote Sens.,* **15,** 3519–3545.

——, D. A. Randall, C. J. Collatz, J. A. Berry, C. B. Field, D. A. Dazlich, C. Zhang, C. D. Collelo, and L. Bounoua, 1996a: A revised land surface parameterization (SiB2) for atmospheric GCMs. Part 1: Model formulation. *J. Climate,* **9,** 676–705.

——, S. O. Los, C. J. Tucker, C. O. Justice, D. A. Dazlich, G. J. Collatz, and D. A. Randall, 1996b: A revised land surface parameterization (SiB2) for atmospheric GCMs. Part 2: The generation of global fields of terrestrial biophysical parameters from satellite data. *J. Climate,* **9,** 706–737.

Shukla, J., and Y. Mintz, 1982: Influence of land-surface evapotranspiration on the Earth's climate. *Science,* **215,** 1498–1500.

——, C. Nobre, and P. Sellers, 1990: Amazon deforestation and climate change. *Science,* **247,** 1322–1325.

Shuttleworth, W. J., 1988: Evaporation from Amazonian rain forest. *Proc. Roy. Soc. London,* **233B,** 321–346.

Sud, Y. C., J. Shukla, and Y. Mintz, 1988: Influence of land surface roughness on atmospheric circulation and precipitation: A sensitivity study with a general circulation model. *J. Appl. Meteor.,* **27,** 1036–1054.

——, G. K. Walker, J.-H. Kim, G. E. Liston, P. J. Sellers, and W. K.-M. Lau, 1996: Biogeophysical consequences of a tropical deforestation scenario: A GCM simulation study. *J. Climate,* **9,** 3225–3247.

Wright, I. R., C. A. Nobre, J. Tomasella, and Coauthors, 1996: Towards a GCM surface parameterization of Amazonia. *Amazonian Deforestation and Climate,* J. H. C. Gash et al., Eds., John Wiley and Sons, 473–504.

Xie, P., and P. A. Arkin, 1997: Global precipitation: A 17-year monthly analysis based on gauge observations, satellite estimates, and numerical model outputs. *Bull. Amer. Meteor. Soc.,* **78,** 2539–2558.

Xue, Y., 1991: A two-dimensional coupled biosphere–atmosphere model and its application. *Adv. Atmos. Sci.,* **8,** 447–458.

——, 1997: Biosphere feedback on regional climate in tropical North Africa. *Quart. J. Roy. Meteor. Soc.,* **123,** 1483–1515.

——, and J. Shukla, 1993: The influence of land surface properties on Sahel climate. Part I: Desertification. *J. Climate,* **6,** 2232–2245.

Zeng, N., and J. D. Neelin, 1999: A land–atmosphere interaction theory for the tropical deforestation problem. *J. Climate,* **12,** 857–872.

——, ——, K.-M. Lau, and C. J. Tucker, 1999: Enhancement of interdecadal climate variability in the Sahel by vegetation interaction. *Science,* **286,** 1537–1547.

——, ——, and C. Chou, 2000: A quasi-equilibrium tropical circulation model—Implementation and simulation. *J. Atmos. Sci.,* **57,** 1767–1796.

Zhang, H., K. McGuffie, and A. Henderson-Sellers, 1996: Impacts of tropical deforestation. Part II: The role of large-scale dynamics. *J. Climate,* **9,** 2498–2521.